

Dynamics of silver nanoparticles in aqueous solution in the presence of metal ions

Kamonwad Ngamchuea, Christopher Batchelor-McAuley, Stanislav V. Sokolov, and Richard G Compton

Anal. Chem., **Just Accepted Manuscript** • DOI: 10.1021/acs.analchem.7b01470 • Publication Date (Web): 08 Sep 2017

Downloaded from <http://pubs.acs.org> on September 8, 2017

Just Accepted

"Just Accepted" manuscripts have been peer-reviewed and accepted for publication. They are posted online prior to technical editing, formatting for publication and author proofing. The American Chemical Society provides "Just Accepted" as a free service to the research community to expedite the dissemination of scientific material as soon as possible after acceptance. "Just Accepted" manuscripts appear in full in PDF format accompanied by an HTML abstract. "Just Accepted" manuscripts have been fully peer reviewed, but should not be considered the official version of record. They are accessible to all readers and citable by the Digital Object Identifier (DOI®). "Just Accepted" is an optional service offered to authors. Therefore, the "Just Accepted" Web site may not include all articles that will be published in the journal. After a manuscript is technically edited and formatted, it will be removed from the "Just Accepted" Web site and published as an ASAP article. Note that technical editing may introduce minor changes to the manuscript text and/or graphics which could affect content, and all legal disclaimers and ethical guidelines that apply to the journal pertain. ACS cannot be held responsible for errors or consequences arising from the use of information contained in these "Just Accepted" manuscripts.



Dynamics of silver nanoparticles in aqueous solution in the presence of metal ions

Kamonwad Ngamchuea, Christopher Batchelor-McAuley, Stanislav V. Sokolov, Richard G. Compton*

* corresponding author: Richard G. Compton, Department of Chemistry, Physical & Theoretical Chemistry Laboratory, University of Oxford, South Parks Road, Oxford, OX1 3QZ, United Kingdom

Email: richard.compton@chem.ox.ac.uk. Tel: +44(0)1865275 957 Fax: +44(0)1865275410

Abstract

Using a combined UV-Vis, DLS and electrochemical approach, this work experimentally studies the physical origin of the observed colorimetric sensitivity of aqueous silver nanoparticles towards divalent metal ions. In the presence of Pb^{2+} , AgNPs are shown to reversibly form agglomerates (the time scale of the reverse de-agglomeration process is of the order of hours). This agglomeration is shown to be induced by complex formation between Pb^{2+} and citrate groups localized on the AgNPs, reducing surface charges (zeta-potential) and hence electrostatic repulsion between the AgNPs. Other divalent metal ions including Ca^{2+} , Cd^{2+} , Zn^{2+} , Ni^{2+} , Co^{2+} and Sn^{2+} are also studied and the resulting sizes of the AgNPs clusters and the extents of the UV-vis spectrum red-shift in λ_{max} have a strong positive correlation with the metal-ligand (citrate) complex formation constant (K_f). This work thus serves as a guide for the selection of capping agents on the basis of K_f and demonstrates the correlation between sizes and spectrophotometric as well as electrochemical responses of the AgNPs clusters. Importantly, we give further physical insights into the size-dependent properties of AgNPs, and emphasize the difference between theoretical and experimental values of extinction coefficients, where the latter is affected by the angle-dependent scattering intensities and the measurement technique used.

Introduction

A plethora of examples of the use of silver nanoparticles for colorimetric and spectrophotometric sensing of metal ions are present in the literature. The most significant variant between these reports is the use of different capping agents. Recent examples include gallic acid,¹ iminodiacetic acid,² ILP,³ tyrosine,⁴ MTT⁵ and biothiols.⁶⁻⁸ Generally, a semi-empirical approach has been taken towards the discovery of new capping agents with the aim of improving the sensitivity and selectivity of the procedure. Nevertheless, we note that most of the ligands previously studied contain either a carboxylate and/or a thiol group, and that in many cases high selectivity towards a specific metal, most often lead (II), is demonstrated. However, many such articles limit themselves to reporting the observed behaviour at the expense of providing insight into the solution phase dynamics of the nanoparticle solution and the probable physico-chemical cause of the altered response.

Silver nanoparticles possess interesting optical properties as their surface plasmon resonance give rise to a strong absorption band in the visible range. The extinction coefficients of the silver nanoparticles ($\epsilon_{\text{per NP}} = 10^8 - 10^{11} \text{ M}^{-1} \text{ cm}^{-1}$)⁹ are several orders of magnitude higher than other types of chromophores,^{10,11} making them ‘ideal’ for colorimetric applications. The colours and absorption spectra of the silver nanoparticles are dependent on their size, shape and the relative permittivity of the local environment. The different absorption spectra of the silver nanoparticles (AgNPs) of different sizes has been well-explored both theoretically and experimentally.^{12,13} The analysis of the absorbance and the extinction coefficients is usually done on the basis of Beer-Lambert law and concentrations are generally described in terms of the particles concentration.⁹ However, it will be demonstrated herein for particles of different sizes that by considering the concentration of *silver atoms* rather than that of silver nanoparticles, insightful and analytically useful information can be obtained. This includes, for example, the discrepancy between the theoretically predicted and experimental UV-Vis spectra, the size-dependent contributions of absorption and scattering in particular.

In sensing applications, the alteration in absorption spectra in response to the change in the relative permittivity becomes of relevant interest. The relative permittivity can change with solvent, the chemical species adsorbed on the surface and the interaction between the particles.¹⁴ It is the latter two factors that draw our attention to the use of AgNPs as a sensor for chemical species. In this work, aqueous *citrate-capped* AgNPs and *lead (II)* are used as a

model system to study the interactions between AgNPs capped with small ligands and the metal ions. Citrate and lead (II) are chosen based on the hypothesis deduced from literature review that lead (II) would give rise to spectrophotometric changes of the AgNPs capped with carboxylate-containing ligands. We note that the behaviour of silver nanoparticles in other solvents *may* differ from that found herein. The investigations into the solution phase dynamics of the AgNPs/lead(II) systems are performed using a range of techniques: UV-Vis spectrophotometry, dynamic light scattering (DLS) and electrochemical nano-impact experiments.^{15,16} The absorption spectra reveal the responses of plasmon resonances and are used to study the reversibility of the interactions. DLS and nano-impacts¹⁵ are employed to monitor the *in-situ* sizes of the particles upon the addition of lead (II) solutions. The *in-situ* techniques allow the monitoring of the size of nanoparticles or nanoparticle clusters in solution-phase, as opposed to transmission electron microscopy (TEM) where the complication of particle agglomeration/aggregation may arise upon solvent evaporation during sample preparation. Based on these techniques, analytical approaches are also developed for the determination of lead (II). Other metal (II) ions are investigated along with the selectivity of the analysis.

Experimental

Chemical reagents and instrumentation

All reagents were used as received without further purification: sodium citrate (Aldrich, 99%), lead (II) nitrate (BDH, 99.5%), calcium nitrate tetrahydrate (BDH, 99.0%), cadmium (II) nitrate tetrahydrate (Aldrich, 99.999%), zinc nitrate hexahydrate (Aldrich, 98%), nickel (II) nitrate hexahydrate (Aldrich, 99.999%), cobalt (II) nitrate hexahydrate (Sigma-Aldrich, >98%), tin (II) chloride (Aldrich, >99.99%), potassium chloride (Sigma-Aldrich, >99.0%). All solutions were prepared using deionized water (Millipore) with a resistivity of 18.2 MΩ cm (25°C).

The UV-Vis measurements were performed with a Shimadzu UV-1800 spectrophotometer in disposable cuvettes (Eppendorf UVette, Sigma-Aldrich) using a 10 mm optical path length. Electrochemical experiments were performed with a μAutolab Type III potentiostat (Utrecht) using a standard three electrode setup employing the fabricated carbon fiber microwire (7 μm

diameter, Goodfellow UK) working electrode,¹⁷ saturated calomel (BASi) reference electrode and a platinum mesh counter electrode.

Synthesis and characterization of citrate-AgNPs

The spherical citrate-AgNPs of 9 nm diameter and the triangular prismatic citrate-AgNPs were synthesized in our research group.¹⁸⁻²⁰ The spherical citrate-AgNPs of 30 nm, 50 nm and 100 nm diameters were obtained from Nanocomposix, USA. All of the citrate-AgNPs were characterized using transmission electron microscopy (TEM, 300 kV JEOL 3000F microscope) and dynamic light scattering (DLS, ZEN3600 Nano-ZS Zetasizer).

Procedures for the analytical detection of Pb²⁺

First, the UV-Vis spectra of 29 nM of 9 nm citrate-AgNPs were recorded in the range of wavelength of 250-800 nm upon the addition of different concentrations of lead nitrate solutions (0–1,000 μM). The position of the wavelength at maximum absorbance (λ_{\max}) and/or the absorbance at 250 nm (A_{250}) are determined and plotted against concentration of Pb²⁺ to construct calibration curves. The concentration of Pb²⁺ in the unknown solution can then be determined by the addition of citrate-AgNPs (yielding the same final concentration of 29 nM) followed by the UV-Vis measurement. The values of λ_{\max} and/or A_{250} measured are then compared with the calibration curves to yield the concentration of Pb²⁺.

Investigations of the interactions between citrate-AgNPs and divalent metal ions

Sizing of citrate-AgNPs/Pb²⁺ clusters. The sizes of the citrate-AgNPs in the presence of different concentrations of Pb²⁺ was determined by DLS and the nano-impacts technique.¹⁵ DLS measurements were performed using 59 nM of 9nm or 7.6 pM of 50nm AgNPs to react with 0, 250, 500, 750 and 1,000 μM of Pb²⁺. Nano-impact experiments were performed in 10 mM KCl electrolytes using 7.6 pM of 50nm citrate-AgNPs in the absence and presence of 1,000 μM of Pb²⁺.

Reversibility. The reversibility of the reaction between citrate-AgNPs and Pb²⁺ was studied by dilution of the mixture of 59 nM 9nm citrate-AgNPs and 1,000 μM Pb²⁺ with deionized water to the dilution factors of 1.5, 2.0 and 2.5. Their UV-Vis spectra are recorded every one minute for the first 7 min, 6 hours and 30 hours after the dilutions. The resulting spectra are

then compared with those expected for the fresh mixtures of AgNPs and Pb^{2+} of equivalent concentrations to that after the dilutions.

Comparison between different divalent metal ions (M^{2+}). In addition to Pb^{2+} , other different metal divalent ions including Ca^{2+} , Cd^{2+} , Zn^{2+} , Ni^{2+} , Co^{2+} and Sn^{2+} were investigated. UV-Vis spectra (250-800 nm) of the mixtures of 7.6 pM 50nm citrate-AgNPs and 500 μM of each metal ion solution were recorded and compared.

Results and Discussion

Given that the main observations for the interaction of silver nanoparticles with metal ions is the change in the colour of the suspension, the article starts by considering the nanoparticle UV-Vis spectra and how the data is best interpreted and analyzed (Section 3.1). Following this, the UV-Vis spectra of the citrate-AgNPs is reported with the addition of different concentrations of lead (II) solutions (Section 3.2). In order to provide insights into the solution phase nanoparticle dynamics in the presence of metal ions, the results from both DLS and the nano-impact technique are presented in Section 3.3. The reversibility of the colour change is investigated in Section 3.4. Finally, Section 3.5 provides an explanation for the observed selectivity of the colour change towards lead (II) ions.

UV-Vis studies of citrate-AgNPs and the interpretation of the resulting spectra

The citrate-AgNPs were characterized using TEM and DLS. Their average sizes are given in Table 1, and the size distributions provided in Figure S1 (SI). Figure 1a presents the UV-Vis spectra of the AgNPs samples ($\lambda = 250\text{-}1,000\text{ nm}$). For the smaller quasi-spherical particles a clear plasmon peak is observable at $\sim 400\text{ nm}$. The large spherical (100 nm) and prismatic particles exhibit shifted absorption maxima. Unlike for molecular species, the extinction coefficient contains contributions from both absorption and scattering. Under conditions where the particle is small compared to the wavelength of light used then under the quasi-static approximation the scattering coefficients, ϵ_{abs} and ϵ_{scatt} can be described as:¹⁴

$$\epsilon_{\text{abs}} = 4\pi Nkr^3 \text{Im}\left[\frac{\epsilon_{\text{in}} - \epsilon_{\text{out}}}{\epsilon_{\text{in}} + 2\epsilon_{\text{out}}}\right] \quad (1),$$

$$\epsilon_{\text{scatt}} = \frac{8}{3} \pi Nk^4 r^6 \left|\frac{\epsilon_{\text{in}} - \epsilon_{\text{out}}}{\epsilon_{\text{in}} + 2\epsilon_{\text{out}}}\right|^2 \quad (2),$$

where ϵ_{abs} and ϵ_{scatt} are absorption and scattering coefficients respectively, and the sum of ϵ_{abs} and ϵ_{scatt} gives ϵ_{ext} ($\epsilon_{\text{ext}} = \epsilon_{\text{abs}} + \epsilon_{\text{scatt}}$). r is the radius of the particles, k is the wavevector in the medium and N is the atomic number density.

First, we note that the scattering is strongly anisotropic, with the fraction of forward scattering increasing with the size of the particle. Second, in a UV-Vis measurement light is made in the forward direction and over a finite range of angles. Consequently, relating theory to the measured UV-Vis spectra, specifically predicting the scattering contribution is not a straight forward task. But we highlight that the absorption coefficient is proportional to the nanoparticle volume, hence for small particles one would anticipate the magnitude of the UV-Vis spectra to relate to the solution phase silver atom concentration. The UV-Vis data presented in Figure 1a has been normalized against the concentration of silver atoms in the suspensions and not the number of particles. For all but the largest particles, the adsorption maxima are very comparable in magnitude. This is the case even though the number of nanoparticles in the four suspensions differs by over two orders of magnitude.

To emphasize this point further, Figure 1b displays the Beer-Lambert plots of absorbance at λ_{max} against concentration of *silver atoms*, with the inlay showing the equivalent plot as a function of *silver nanoparticles* concentration. The Beer-Lambert plots vs. silver nanoparticles are markedly different for the nanoparticles of different sizes. The resulting values of ϵ_{ext} per NP are provided in Table 1. The values of ϵ_{ext} calculated using the concentrations of *silver atoms* are in the range of $15,300 \pm 300$ (Ag atom) $\text{M}^{-1} \text{cm}^{-1}$, refer to Table 1. The slightly different values of ϵ_{ext} possibly reflect the errors in the concentrations of silver used in the synthesis. Only the 100 nm AgNPs have ϵ_{ext} an order of magnitude lower than the smaller particles.

Given that Evanoff et al.¹² reports that for silver nanoparticles scattering and absorption contribute equally to the extinction coefficient when particles are ca. 52 nm in size, it is of interest to ask why the adsorption maxima for the reported 50 nm particles exhibit a very comparable measured extinction coefficient to the much smaller 9 nm particles (on a per atom basis). Again we emphasize that the measured spectra are highly dependent on the technique used. In the case of UV-Vis which is a widely-used method among analytical chemists, the detector is placed in front of the sample or at the scattering angle (θ) of $\sim 0^\circ$. For small particles the scattering intensities are maximum for forward ($\theta = 0^\circ$) and backward ($\theta = 180^\circ$) scattering, and minimum at the perpendicular angle ($\theta = 90^\circ$).²¹ The light scattered in

the other directions except for $\theta = 0^\circ$ is not detected by the detector, and hence increases the magnitude of ‘absorbance’ measured by the UV-Vis.

In contrast, as the particle size becomes comparable to the wavelength of light such as the 100 nm AgNPs studied, scattering now gives the highest intensity in the forward direction ($\theta = 0^\circ$).²¹ More scattered light reaches the detector and decreases the value of ‘absorbance’ measured by the UV-Vis. The extinction coefficient from the UV-Vis measurement is thus significantly lower than anticipated for the smaller size particles. This result emphasizes the difference between experimental and theoretical values of extinction coefficients. Nonetheless, from our work it is suggested that for AgNPs not larger than 50 nm in diameter, the UV-Vis maximum absorbance can be analyzed using the Beer-Lambert law using the value of ϵ_{ext} per silver atom of $15,300 \pm 300$ (Ag atom) $\text{M}^{-1} \text{cm}^{-1}$. The value of ϵ_{ext} per silver nanoparticle can also be approximated, see S2 (SI).

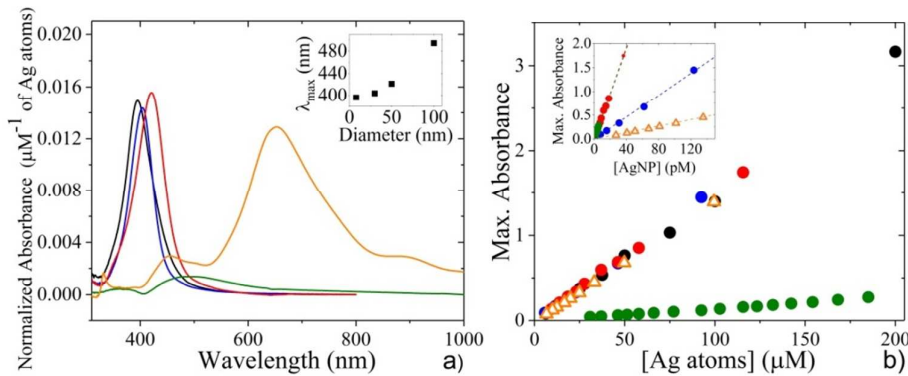


Figure 1: a) UV-Visible spectra of citrate-AgNPs of different sizes normalized with the concentrations of silver atoms; (Inlay) the wavelengths at maximum absorbance (λ_{max}) as a function of the AgNPs diameters. b) Beer-Lambert plots of absorbance at λ_{max} as a function of *silver atoms* concentrations and (Inlay) absorbance at λ_{max} as a function of *silver nanoparticles* concentrations for citrate-AgNPs of different shapes and sizes. **Black, blue, red and green** designate spherical citrate-AgNPs of 9 nm, 30 nm, 50 nm and 100 nm in diameter respectively; orange designates triangular-prism citrate-AgNPs of 33 nm triangular height and 7 nm prism thickness.

Table 1: Sizes of citrate-AgNPs from TEM and DLS measurements, and the extinction coefficients (ϵ) calculated on the basis of Beer-Lambert law using silver nanoparticle or silver atom concentrations.

*	TEM diameter (nm)	DLS z-average (nm)	ϵ per AgNP ($10^{11} \text{ M}^{-1} \text{ cm}^{-1}$)	ϵ per Ag atom ($\text{M}^{-1} \text{ cm}^{-1}$)
[1]	9 ± 2	18 ± 12	3.34 ± 0.03	$15,460 \pm 220$
[2]	29 ± 4	39 ± 9	634 ± 2	$15,520 \pm 150$
[3]	47 ± 6	60 ± 11	$2,580 \pm 4$	$14,995 \pm 95$
[4]	103 ± 9	111 ± 11	$2,586 \pm 2$	$1,445 \pm 35$
[5]	$h: 33 \pm 9^\dagger$ $l: 7 \pm 1^{19}$	25 ± 15	344 ± 1	$13,980 \pm 190$

* [1] spherical (made in house),¹⁸ [2] spherical (Nanocomposix, Nanoxact 30 nm), [3] spherical (Nanocomposix, Nanoxact 50 nm), [4] spherical (Nanocomposix, Nanoxact 100 nm), [5] triangular prisms (made in house)¹⁹

\dagger h and l are the height of the triangular surface and the thickness of the prism respectively.

UV-Vis responses of the citrate-AgNP/Pb²⁺ solutions

In this section, the optical properties and the UV-Vis responses of the citrate-AgNPs are investigated upon additions of Pb²⁺ solutions. The absorption spectra are recorded for the mixtures of citrate-AgNPs (58 nM of 9 nm AgNPs or 7.6 pM of 50 nm AgNPs) and Pb²⁺ (0-1,000 μM). The resulting UV-Vis spectra are presented in Figure 2a and 2d for 9 nm and 50 nm AgNPs respectively. Two distinct features are observed to change with the concentrations of Pb²⁺ added: the absorbance at $\lambda = 250$ nm (A_{250}) and the positions of λ_{\max} . A_{250} increases with Pb²⁺ concentrations, while λ_{\max} shifts to longer wavelengths, both changes of which are plotted against the concentrations of Pb²⁺ in Figure 2b and 2e for 9 nm and 50 nm AgNPs respectively.

In the case of 9 nm AgNPs in the presence of 200 μM and 300 μM Pb²⁺, the spectra in the region of 350 – 600 nm split into two peaks, which are labelled Peak I and Peak II. The magnitude of the maximum absorbance, or the sum of absorbance at Peak I and Peak II if there are two separate peaks, remains constant with Pb²⁺ concentrations, indicating the relation of the spectra in this region to the amount of silver, see Figure 2c and 2f for 9 nm and 50 nm AgNPs respectively. Note that the slightly higher maximum absorbance at high Pb²⁺ concentrations, especially for the 50 nm AgNPs, is caused by the interference of the absorbance due to the citrate-Pb²⁺ complex (A_{250}) which will be discussed in Section 3.5.

Further results on the effects of concentrations of citrate-AgNPs, and electrolytes towards the detection of lead ions are provided in section S3 (SI). The change in colour is presented in Figure S4 (SI). The lowest limits of detection were obtained when 29 nM of 9 nm citrate-AgNPs were used (Figures S2a and S2b), yielding the limits of detection ($3S_B/m$) of 35 μM and 18 μM based on λ_{\max} and A_{250} respectively. From the limits of detection determined, it is suggested that the developed method may be suitable for the determination of Pb²⁺ in industrial wastewater where the concentration of Pb²⁺ are in the range of 5-15 mg/L (24.1 μM to 72.4 μM).²²

This shift in the UV-Vis response and the change in colour of the nanoparticle suspension in the presence of Pb²⁺ demonstrates that the AgNPs capped with carboxylate-containing ligands (citrate in this case) chemically interact. Having demonstrated that we can obtain analytically useful information from the interactions between citrate-AgNPs and Pb²⁺ as

previously reported for other capping agents,¹⁻⁸ next we investigate the cause of the changes in absorption spectra.

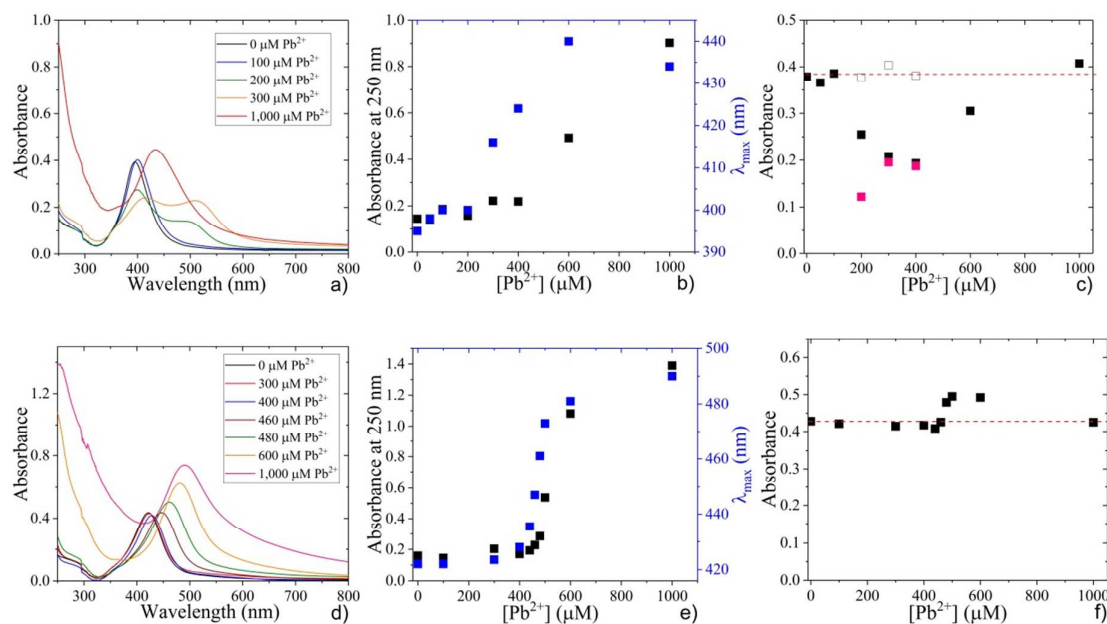


Figure 2: a) UV-Vis spectra, b) (black) absorbance at 250 nm and (blue) λ_{max} plotted against concentrations of Pb^{2+} , and c) absorbance at (black squares) λ_{max} or Peak I if spectra split into two peaks, (pink squares) Peak II, (open squares) sum of absorbance at Peak I and Peak II of the mixtures of 58 nm 9 nm citrate-AgNPs and 0-1,000 μM of Pb^{2+} . d) UV-Vis spectra, e) (black) absorbance at 250 nm and (blue) λ_{max} plotted against concentrations of Pb^{2+} and f) absorbance at λ_{max} of the mixtures of 7.6 pM 50 nm citrate-AgNPs and 0-1,000 μM of Pb^{2+} .

Solution phase dynamics of the citrate-AgNP/ Pb^{2+} solutions – evidencing the formation of AgNPs clusters

It is thought that the plasmon resonance of the particles and hence the resulting absorption spectra change according to three main factors: solvents, formation of AgNP clusters and adsorption of Pb^{2+} on the surface of the AgNPs. The only change made to the solvent is the addition of low concentrations of Pb^{2+} which is approximated from the resemblance of the UV-Vis spectra of Pb^{2+} solution and pure water to cause a negligible effect on the relative permittivity of the medium. Consequently, in this section we focus on the possible formation of AgNP clusters in Pb^{2+} solutions. The sizes of the AgNPs in the presence of different concentrations of Pb^{2+} are determined using two *in-situ* techniques: dynamic light scattering and the electrochemical nano-impacts technique.

The hydrodynamic sizes of the AgNPs in the presence of 0, 250, 500 and 1,000 μM Pb^{2+} from DLS measurements are summarized in Table 2. The average sizes of the particles become significantly larger in the presence of Pb^{2+} , and the size increases with increasing

Pb^{2+} concentration. These results thus indicate the formation of AgNP clusters induced by Pb^{2+} .

Table 2: DLS sizes of the nanoparticles in the presence of different concentrations of Pb^{2+} in the absence of added electrolytes. Similar experiments were performed in the presence of 10 mM KCl, the results of which are provided in Section S5 in the SI.

$[\text{Pb}^{2+}]$ (μM)	AgNPs d = 8 nm z-average (nm)	AgNPs d = 50 nm z-average (nm)
0	18 ± 12	52 ± 2
250	125 ± 33	59 ± 11
500	291 ± 63	157 ± 12
750	457 ± 103	381 ± 82
1000	639 ± 157	870 ± 152

Nano-impact experiments are also performed to confirm the cluster formation of the NPs in the presence of Pb^{2+} and obtain further information about the nature of the clusters. The potential of 0.8 V vs SCE is applied at a carbon fiber working electrode and the currents monitored as a function of time. The electrochemical measurements are performed in 10 mM KCl supporting electrolyte to provide sufficient screening of the positively charged Ag^+ oxidation product, and hence ensure complete oxidation of the AgNPs.²³ The examples of nano-impact *spikes* are given in Figure 3.

Figure 3a displays the typical sharp spikes of AgNPs, where each spike represents a AgNP being completely oxidized at the electrode, giving the charge transfer of 0.48 ± 0.23 pC in the duration of 18 ± 5 ms. These amounts of charge transfer correspond to the diameters of AgNPs of 45 ± 8 nm, in excellent agreement with the size from TEM measurements of 47 ± 6 nm. The detailed analysis of nano-impact spikes are provided in Section S6 (SI).

In the presence of 1,000 μM Pb^{2+} , the duration of spikes becomes significantly longer (719 ± 621 ms) indicating the much larger sizes of the particles as longer times are required for the large particles to be fully oxidized, see Figure 3b. The charge transfer is determined to be 174 ± 173 pC, corresponding to 297 ± 101 nm diameters assuming the clusters are spherical. Importantly, the detectable nano-impact spikes of the AgNPs clusters further demonstrates that the interacting forces between the clusters are relatively strong, and that if the formation of clusters is reversible, the disassembly of the clusters is much slower than the oxidation of AgNPs upon the *impact* on the electrode.^{24,25} Otherwise, only monomeric NPs would be detected.²⁶

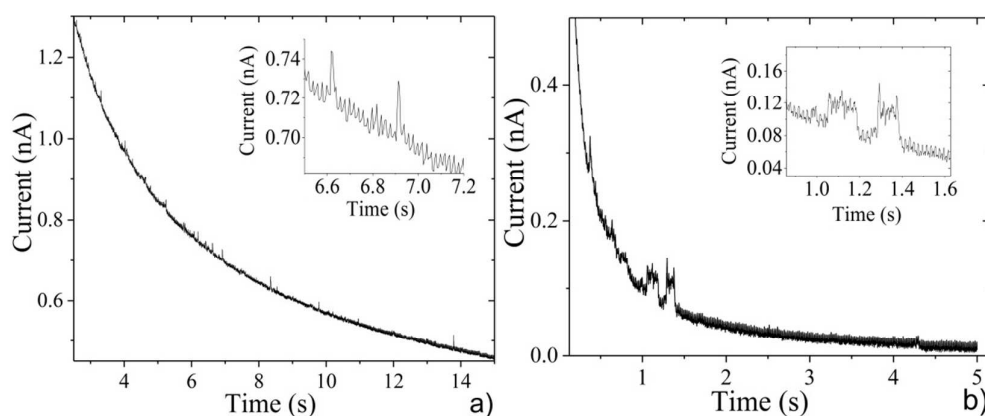


Figure 3: Chronoamperograms showing nano-impact spikes of a) 7.6 pM of 50 nm AgNPs and b) 7.6 pM of 50 nm AgNPs in the presence of 1,000 μM Pb^{2+} using 7 μm carbon fiber working electrode, standard calomel reference electrode and platinum counter electrode, $E = 0.8$ V vs SCE, 10 mM KCl supporting electrolyte.

Reversibility of the AgNPs cluster formation in Pb^{2+} solutions - Agglomeration vs. Aggregation

The previous section has evidenced that the addition of Pb^{2+} to AgNPs suspension results in the formation of the AgNPs clusters. In this section, it is investigated whether this cluster formation is an agglomeration (reversible) or aggregation (irreversible) process.²⁷ This was achieved by mixing 58 nM of 9 nm AgNPs and 1,000 μM Pb^{2+} . The mixture is then diluted with deionized water to the dilution factors of 1.5, 2.0 and 2.5 yielding 39 nM AgNP/667 μM Pb^{2+} , 29 nM AgNP/500 μM Pb^{2+} and 23 nM AgNP/400 μM Pb^{2+} respectively. The UV-Vis spectra of the diluted mixtures are recorded and compared with the mixtures prepared *fresh* to the equivalent concentrations of AgNPs and Pb^{2+} . Figure 4 demonstrates the results for the dilution factors of 2.5 showing the shape of the UV-Vis spectra returning gradually to that expected for the 23 nM AgNP/400 μM Pb^{2+} mixtures. The time scale of the reverse process is determined based on the ratios between the absorbance at 405 nm to 517 nm to be of the order of hours. Further results are provided in Section S7 (SI).

From this result, it can thus be concluded that the interaction with Pb^{2+} leads to the *reversible agglomeration* of the AgNPs, with slow de-agglomeration process. The slow rate of the de-agglomeration establishes credibility in the determination of metal ions based on the sizes of the nanoparticles clusters as it ensures that no cluster de-agglomerates in the timescale of the measurement. The reversibility of the agglomeration also suggests the possible re-use of the nanoparticles in analysis as there is no irreversible loss. However due to the reversibility of the agglomeration process, in the extreme cases where a separation process is required and

the process takes a significant period of time, the measured responses may not truly reflect the concentrations of the metal ions in the samples, and caution should be exercised.

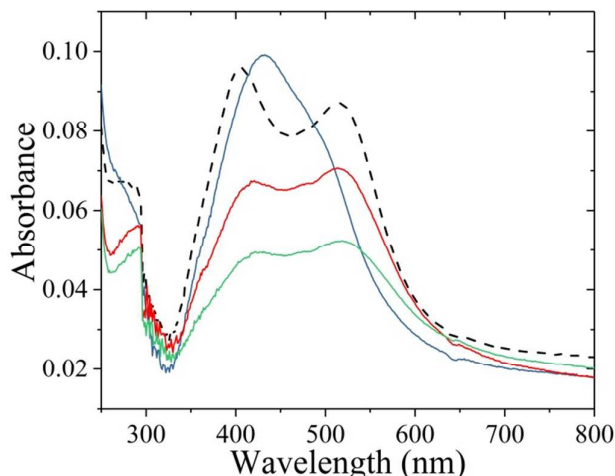


Figure 4: UV-Vis spectra of the mixtures of 23 nM AgNP/400 μM Pb^{2+} yielding from the dilution of 58 nM of 9 nm AgNPs and 1,000 μM Pb^{2+} to the dilution factor of 2.5. Blue, red and green lines designate the spectra of the diluted mixtures 7 min, 6 hr and 30 hr after dilution respectively. Black dashed line shows the spectrum of fresh 23 nM AgNP/400 μM Pb^{2+} mixtures, i.e. not from dilution.

Origins of the reversible agglomeration

In this section, the physical origins of the agglomeration of citrate-AgNPs in the presence of Pb^{2+} are examined. Figure 5 compares the UV-Vis spectra of the mixtures of Pb^{2+} and citrate-AgNPs, with that of Pb^{2+} and the solution-phase citrate. The spectra display strong absorbance at 250 nm (A_{250}) which is absent prior to the mixing between Pb^{2+} and any form of citrate. This indicates complex formation between Pb^{2+} and citrates, both in solution-phase and as ligands bound to the surface of AgNPs. Citrate contains three carboxylate groups and likely binds to Pb^{2+} via the oxygen/carbonyls of the carboxylate groups.²⁸ The Pb-O^{29} and the Pb-OOC interaction in ethylenediaminetetraacetic acid (EDTA)³⁰ have been reported to display strong absorption in this short wavelength region.

Monolayer adsorption of citrate on gold nanoparticles is ca. $2.8 \times 10^{-10} \text{ mol cm}^{-2}$, the number of which is also applicable to the silver surface as it has similar lattice spacings.³¹ For 15.1 pM of the commercial (Nanocomposix) 50 nm citrate-AgNPs, the suspension contains 625 μM citrate, <1% of which is localized on the AgNPs while >99% remains in the solution. For the mixtures of 15.1 pM 50 nm citrate-AgNPs (containing 625 μM citrate) and 1,000 μM Pb^{2+} , the magnitude of A_{250} is significantly higher than that of the mixture of Pb^{2+} with the same concentration of citrate in solution. At the same time, the absorption spectrum in the 250-350 nm range of the Pb^{2+} /solution-phase citrate mixture only becomes comparable to that

of 15.1 pM 50 nm citrate-AgNPs (containing 625 μM citrate) and 1,000 μM Pb^{2+} when the concentration of Pb^{2+} is increased to 2,000 μM . The higher amount of Pb^{2+} required to reach a comparable magnitude as that of the citrate-AgNPs of equivalent citrate concentration implies that the AgNPs act as the carriers of the citrate, localizing high concentrations of citrate on the surface. This likely facilitates the complex formation and hence improves the sensitivity of the detection of Pb^{2+} .

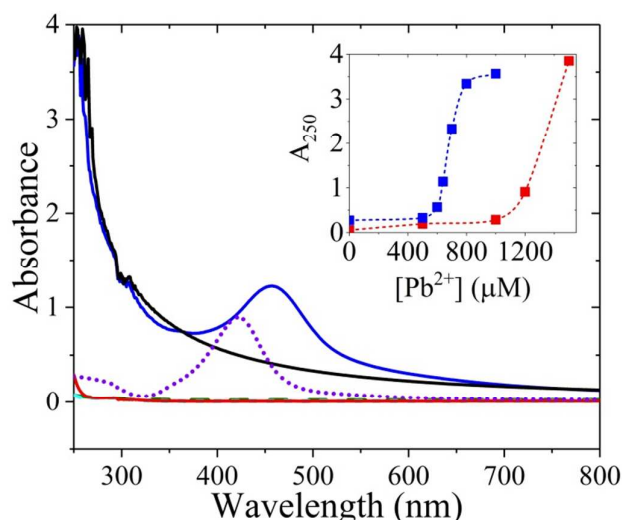


Figure 5: UV-Vis spectra of (Dashed, green) 625 μM citrate; (Dashed, light blue) 1,000 μM Pb^{2+} (overlay on top of the dashed green line); (Dotted, purple) 15.1 pM 50 nm citrate-AgNPs; (Red) 1,000 μM Pb^{2+} + 625 μM citrate; (Black) 2,000 μM Pb^{2+} + 625 μM citrate; (Blue) 1,000 μM Pb^{2+} + 15.1 pM 50 nm citrate-AgNPs (containing 625 μM citrate; >99% in solution and the remaining localized on the nanoparticles). (Inlay) Calibration curves showing the absorbance at 250 nm (A_{250}) as a function Pb^{2+} concentration interacting with (Blue) 15.1 pM 50 nm citrate-AgNPs (containing 625 μM citrate) or (Red) 625 μM citrate

The zeta potentials of the citrate-AgNPs are measured to be -23.3 ± 1.8 mV and -10.0 ± 0.2 mV in the absence and presence of 750 μM Pb^{2+} respectively, see Section S8 (SI) for raw data. The decrease in the surface charges reduces the electrostatic repulsion, and leads to the agglomeration of the AgNPs. The Pb^{2+} ion can also potentially act as a bridge between nanoparticles to form agglomerates. The modification made to the surface environment and the agglomeration of the NPs (decreasing particles separation) alter the plasmon resonance frequency, shifting the position of the absorption peak to longer wavelengths upon the binding of Pb^{2+} .

In addition to Pb^{2+} , the UV-Vis spectra and DLS measurements were performed for the mixtures of 7.6 pM of 50 nm citrate-AgNPs and 500 μM of different divalent cations (Ca^{2+} , Cd^{2+} , Zn^{2+} , Ni^{2+} , Co^{2+} and Sn^{2+}). Mono- and other multi-valent cations are not considered in

this work to eliminate the complication arising from different ionic strengths. The resulting values of A_{250} and $\Delta\lambda_{\max}$ are summarized in Table 3, together with the formation constants (K_f) of the citrate- M^{2+} complexes. The raw spectra are given in Section S9 (SI).

The complex formation constant (K_f) is defined as:



where M^{2+} and $[M\text{-Citrate}]^-$ are divalent metal cations and the metal-citrate complex respectively. $K_f = [M\text{-Citrate}]^- / [M^{2+}][\text{Citrate}^{3-}]$.

As shown in Table 3, both the sizes of the particles and $\Delta\lambda_{\max}$ increase with K_f . At the same concentration, M^{2+} with higher K_f values form higher concentrations of the $[M\text{-Citrate}]^-$ complex. Consequently, more significant change is likely made to the nanoparticle surface dielectric constant. At the same time, the complex formation between M^{2+} and citrate leads to the decrease in zeta-potential, and hence agglomeration. Both the localization of Pb^{2+} on the surface of AgNPs and the decrease in the particle separation may give rise to *strong near-field coupling*,¹⁴ developing a large charge dipole across the gap between the particles and hence changing the frequency of the plasmon resonance.

Apart from the carboxylate-containing ligands (such as citrate), AgNPs localized with biothiols also show high selectivity towards Pb^{2+} .⁶⁻⁸ Crea et al.³² report that the complex formation between Pb^{2+} and biological S-donor ligands have the high $\log(K_f)$ values of greater than 10, and hence further support the inference that the selectivity in the metal ion detection by silver nanoparticles is governed by the magnitude of K_f of metal-ligand binding.

Both Pb^{2+} and Sn^{2+} have high $\log(K_f)$ values for citrate complex formation and both show significant shifts in λ_{\max} and form large agglomerates. However, $\Delta\lambda_{\max}$ of citrate-AgNPs in the presence of Sn^{2+} is smaller than that in Pb^{2+} solutions, suggesting that although K_f is dominant, it may not be a sole factor. This is thought to be a result of the larger size of Pb^{2+} allowing the formation of complexes with higher coordination number. Nonetheless, the knowledge of K_f dependence on the size of AgNPs clusters and the shift in plasmon resonance in M^{2+} solutions allows the bottom-up design of the nanoparticle sensors, and the selection of the capping ligands in particular. This work indicates that capping ligands can be chosen on the basis of complex formation constant with the target analytes.

Table 3: Literature values of metal-citrate complex formation constants (K_f); UV-Vis experimental values of absorbance at 250 nm (A_{250}) and $\Delta\lambda_{\max}$ for the mixtures of 7.6 pM 50 nm citrate-AgNPs and 500 μ M of different M^{2+} .

M ²⁺	Metal-citrate complex formation constant (K _f)				A ₂₅₀	Δλ _{max} (nm)	DLS z-average (nm)
	log(K _f)		average log(K _f) values				
Ca ²⁺	4.9 ^{33,34}	3.15 ³⁵	4.84 ³⁶	4.30 ± 0.99	0.09	1	64
Cd ²⁺	4.2 ³⁷	3.98 ³⁸		4.09 ± 0.16	0.10	0	59
Zn ²⁺	3.55 ³⁹	4.85 ³⁸	4.71 ⁴⁰	4.37 ± 0.71	0.14	2	59
Ni ²⁺	5.11 ³⁸	4.47 ⁴¹	4.99 ⁴²	4.86 ± 0.34	0.12	1	57
Co ²⁺	4.83 ³⁸	4.16 ⁴³	4.41 ⁴²	4.47 ± 0.34	0.16	1	60
Pb ²⁺	5.74 ⁴⁴	6.5 ⁴⁴		6.12 ± 0.54	0.21	22.5	157
Sn ²⁺	19.5 ⁴⁵	10.3 ⁴⁶		14.90 ± 4.60	0.37	15	1,036

References to the values of $\log(K_f)$ can also be found in Stability Constants (Special Publication No. 17).⁴⁷

Conclusions

We have examined the physical origins underlying the interactions between AgNPs capped with small ligands and the metal ions in aqueous solution (the extension of these result to other media and conditions warrants further investigation). The interactions which give rise to the changes in optical and spectrophotometric responses of the AgNPs are found to be due to the reversible agglomeration of the particles caused by the complex formation between the metal ions and the capping agents. The complex formation reduces the zeta-potential of the particles and hence leads to particle agglomeration. The sizes of the agglomerates and the shift in the plasmon resonance frequency are governed by the strength of the metal ion-capping agent complex. This work thus provides evidences and physical explanation to facilitate the choice of capping agent selection (based on K_f) for the detection of the species of interest. We have also shown that the analytical detection of metal ions, using lead (II) as an example, can be done on the basis of optical, spectrophotometric, dynamic light scattering or electrochemical nano-impact measurements of the AgNPs suspensions.

Acknowledgements

We thank Ms. Jessica Lee for the synthesis of silver nanoparticles. KN acknowledges funding from DPST scholarship, the Royal Thai government. This project is supported by the funding from the European Research Council under the European Union’s Seventh Framework Programme (FP/2007-2013)/ERC Grant Agreement no. [320403].

Supporting Information

TEM images of citrate-AgNPs; calculations of ϵ_{ext} ; UV-Vis spectra and change in colours of citrate-AgNPs upon the addition of Pb^{2+} ; effect of electrolytes; nano-impacts; reversibility of the agglomeration; zeta-potential of citrate-AgNPs in the absence and presence of Pb^{2+} ; binding of citrate-AgNPs to different divalent cations

References

- (1) Yoosaf, K.; Ipe, B. I.; Suresh, C. H.; Thomas, K. G. *J. Phys. Chem. C* **2007**, *111*, 12839-12847.
- (2) Qi, L.; Shang, Y.; Wu, F. *Microchim. Acta* **2012**, *178*, 221-227.
- (3) Vinod Kumar, V.; Anthony, S. P. *Sens. Actuators, B* **2014**, *191*, 31-36.
- (4) Annadhasan, M.; Muthukumarasamyvel, T.; Sankar Babu, V. R.; Rajendiran, N. *ACS Sustainable Chem. Eng.* **2014**, *2*, 887-896.
- (5) Noh, K. C.; Nam, Y. S.; Lee, H. J.; Lee, K. B. *Analyst* **2015**, *140*, 8209-8216.
- (6) Anambiga, I. V.; Suganthan, V.; Arunai Nambi Raj, N.; Buvaneswari, G.; Sampath Kumar, T. S. *IJSER* **2013**, *4*, 710.
- (7) Hu, L.; Hu, S.; Guo, L.; Tang, T.; Yang, M. *Anal. Methods* **2016**, *8*, 4903-4907.
- (8) Chen, X.; Cheng, X.; Gooding, J. J. *Analyst* **2012**, *137*, 2338-2343.
- (9) Paramelle, D.; Sadovoy, A.; Gorelik, S.; Free, P.; Hobley, J.; Fernig, D. G. *Analyst* **2014**, *139*, 4855-4861.
- (10) Chen, H.; Huang, H.; Huang, X.; Clifford, J. N.; Forneli, A.; Palomares, E.; Zheng, X.; Zheng, L.; Wang, X.; Shen, P.; Zhao, B.; Tan, S. *J. Phys. Chem. C* **2010**, *114*, 3280-3286.
- (11) Choi, H.; Raabe, I.; Kim, D.; Teocoli, F.; Kim, C.; Song, K.; Yum, J. H.; Ko, J.; Nazeeruddin, M. K.; Gratzel, M. *Chem. - Eur. J.* **2010**, *16*, 1193-1201.
- (12) Evanoff, D. D.; Chumanov, G. *J. Phys. Chem. B* **2004**, *108*, 13957-13962.
- (13) Félidj, N.; Aubard, J.; Lévi, G. *J. Chem. Phys.* **1999**, *111*, 1195-1208.
- (14) Pelton, M.; Bryant, G. W. *Introduction to Metal-Nanoparticle Plasmonics*; Wiley: New York, 2013.
- (15) Sokolov, S. V.; Eloul, S.; Katelhon, E.; Batchelor-McAuley, C.; Compton, R. G. *Phys. Chem. Chem. Phys.* **2017**, *19*, 28-43.
- (16) Cheng, W.; Compton, R. G. *TrAC, Trends Anal. Chem.* **2014**, *58*, 79-89.
- (17) Ellison, J.; Batchelor-McAuley, C.; Tschulik, K.; Compton, R. G. *Sens. Actuators, B* **2014**, *200*, 47-52.
- (18) Lees, J. C.; Ellison, J.; Batchelor-McAuley, C.; Tschulik, K.; Damm, C.; Omanovic, D.; Compton, R. G. *ChemPhysChem* **2013**, *14*, 3895-3897.
- (19) Bartlett, T. R.; Sokolov, S. V.; Plowman, B. J.; Young, N. P.; Compton, R. G. *Nanoscale* **2016**, *8*, 16177-16181.
- (20) Jin, R.; Cao, Y.; Mirkin, C. A.; Kelly, K. L.; Schatz, G. C.; Zheng, J. G. *Science* **2001**, *294*, 1901-1903.
- (21) Bohren, C. F.; Huffman, D. R. *Absorption and scattering of light by small particles*; Wiley: New York, 1983.
- (22) Sheng, P. X.; Ting, Y. P.; Chen, J. P.; Hong, L. *J. Colloid Interface Sci.* **2004**, *275*, 131-141.
- (23) Krause, K. J.; Brings, F.; Schnitker, J.; Katelhon, E.; Rinklin, P.; Mayer, D.; Compton, R. G.; Lemay, S. G.; Offenhausser, A.; Wolfrum, B. *Chem. - Eur. J.* **2017**, *23*, 4638-4643.
- (24) Ellison, J.; Tschulik, K.; Stuart, E. J.; Jurkschat, K.; Omanovic, D.; Uhlemann, M.; Crossley, A.; Compton, R. G. *ChemistryOpen* **2013**, *2*, 69-75.
- (25) Sokolov, S. V.; Tschulik, K.; Batchelor-McAuley, C.; Jurkschat, K.; Compton, R. G. *Anal. Chem.* **2015**, *87*, 10033-10039.
- (26) Bartlett, T. R.; Sokolov, S. V.; Holter, J.; Young, N.; Compton, R. G. *Chem. - Eur. J.* **2016**, *22*, 7408-7414.

- (27) Alemán, J. V.; Chadwick, A. V.; He, J.; Hess, M.; Horie, K.; Jones, R. G.; Kratochvíl, P.; Meisel, I.; Mita, I.; Moad, G.; Penczek, S.; Stepto, R. F. T. *Pure Appl. Chem.* **2007**, 79.
- (28) Kourgiantakis, M.; Matzapetakis, M.; Raptopoulou, C. P.; Terzis, A.; Salifoglou, A. *Inorg. Chim. Acta* **2000**, 297, 134-138.
- (29) Arulmozhi, K. T.; Mythili, N. *AIP Advances* **2013**, 3, 122122.
- (30) Welcher, F. J. *The Analytical Uses of Ethylenediamine Tetraacetic Acid*; Van Nostrand, 1958.
- (31) Park, J. W.; Shumaker-Parry, J. S. *J. Am. Chem. Soc.* **2014**, 136, 1907-1921.
- (32) Crea, F.; Falcone, G.; Foti, C.; Giuffrè, O.; Materazzi, S. *New J. Chem.* **2014**, 38, 3973.
- (33) Davies, C. W.; Hoyle, B. E. *J. Chem. Soc.* **1953**, 4134.
- (34) Bates, R. G.; Pinching, G. D. *J. Am. Chem. Soc.* **1949**, 71, 1274-1283.
- (35) Schubert, J. *J. Am. Chem. Soc.* **1954**, 76, 3442-3444.
- (36) Heinz, E. *Biochem. Z.* **1951**, 321, 314.
- (37) Meites, L. *J. Am. Chem. Soc.* **1951**, 73, 3727-3731.
- (38) Li, N. C.; Lindenbaum, A.; White, J. M. *J. Inorg. Nucl. Chem.* **1959**, 12, 122-128.
- (39) Korshunov, I. A.; P., P. A.; Tikhomirova, V. M. *Zhur. neorg. Khim.* **1957**, 2, 68.
- (40) Schubert, J.; Lind, E. L.; Westfall, W. M.; Pfleger, R.; Li, N. C. *J. Am. Chem. Soc.* **1958**, 80, 4799-4802.
- (41) Heitner, C.; Friedmann, D.; Goldschmidt, J. H.; Shamin, J. *Bull. Soc. Chim. France* **1958**, 864.
- (42) Migal, P. K.; Sycheu, A. Y. *Zhur. neorg. Khim.* **1958**, 3, 314.
- (43) Li, N. C.; Westfall, W. M.; Lindenbaum, A.; White, J. M.; Schubert, J. *J. Am. Chem. Soc.* **1957**, 79, 5864-5870.
- (44) Kety, S. S. *J. Biol. Chem.* **1942**, 142, 181.
- (45) Survila, A.; Mockus, Z.; Kanapeckait, S. *Electrochim. Acta* **2000**, 46, 571-577.
- (46) Tselesh, A. S. *Thin Solid Films* **2008**, 516, 6253-6260.
- (47) Lars Gunnar, S.; Arthur, M. E. *Stability Constants of Metal-ion Complexes*; London Chemical Society, 1964.

For TOC only

